International Journal of Pharmaceutics: X 8 (2024) 100288

Contents lists available at ScienceDirect

International Journal of Pharmaceutics: X

journal homepage: www.sciencedirect.com/journal/international-journal-of-pharmaceutics-x

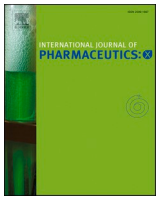

Effect of wound dressing porosity and exudate viscosity on the exudate absorption: *In vitro* and *in silico* tests with 3D printed hydrogels

Alejandro Seijo-Rabina [a,1], Santiago Paramés-Estevez [b,c,1], Angel Concheiro [a], Alberto Pérez-Muñuzuri [b,c], Carmen Alvarez-Lorenzo [a,*]

[a] *Departamento de Farmacología, Farmacia y Tecnología Farmacéutica, I+D Farma (GI-1645), Facultad de Farmacia, Instituto de Materiales (iMATUS) and Health Research Institute of Santiago de Compostela (IDIS), Universidade de Santiago de Compostela, 15782 Santiago de Compostela, Spain*
[b] *Group of NonLinear Physics, Universidade de Santiago de Compostela, 15782 Santiago de Compostela, Spain*
[c] *Galician Center for Mathematical Research and Technology (CITMAga), 15782 Santiago de Compostela, Spain*

A R T I C L E I N F O

Keywords:
Wound dressing
3D printed hydrogel
Exudate absorption
Viscosity
Computational modeling
Pore size

A B S T R A C T

Exudate absorption is a key parameter for proper wound dressing performance. Unlike standardized tests that consider exudate viscosity close to that of water, patients' exudates vary greatly in composition and, therefore, viscosity. This work aimed to investigate the effects of exudate viscosity and pore size of hydrogel-like dressings on the exudate absorption rate to establish rational criteria for the design of dressings that can meet the personalized needs of wound treatment. Computer-aided design (CAD) was used for Digital Light Processing (DLP) 3D printing of hydrogels with 0%, 30% and 60% porosity. The hydrogels were characterized in detail, and the absorption of two simulated exudate fluids (SEFs) was video-recorded. The same CAD files were used to develop *in silico* models to simulate exudate uptake rate. Both *in vitro* data and *in silico* modeling revealed that low-viscosity SEF penetrates faster through relatively small hydrogel pores (approx. 400 μm) compared to larger pores (approx. 1100 μm) due to capillary forces. However, *in vitro* vertical uptake took longer than when simulated using CAD design due to lateral fluid absorption through the pore walls in the hydrogel bulk. Distortions of hydrogel channels (micro-CT images) and lateral fluid absorption should be both considered for *in silico* simulation of SEF penetration. Overall, the results evidenced that porous hydrogel dressings allow rapid penetration (within a few seconds) and hosting of exudates, especially for pore size <1 mm. This information may be useful for design criteria of wound dressings with adequate fluid handling and drug release rate.

1. Introduction

Wound exudate is defined as a water-based leakage from capillaries. Its composition varies depending on the exudate production, wound healing stage, infection, chronicity of the injury and patient conditions (pathologies). The composition of the exudate is a mixture of proteins, cells involved in the healing process, enzymes, glucose, bacteria secretions (if the case) and waste products (WUWHS, 2007; Ruf et al., 2017). When an injury occurs, the inflammatory stage begins with the arrival of inflammatory mediators, and the permeability of the capillaries increases allowing the excess fluid to arrive at the wound site (Vowden and Vowden, 2003). The role of the exudate is to support the healing by preventing the wound from drying out, contributing to cell migration, providing cell nutrition, allowing diffusion of immune and growth factors, and helping the autolysis (Lustig et al., 2021). In the normal healing process the exudate is a necessary element; however, in chronic and/or infected wounds, the abnormal production of exudate and the variations in the components concentration may delay the healing or worsen the injury (Tickle, 2016; Townsend et al., 2024).

Chronic wounds are characterized by a prolonged inflammatory stage and, therefore, an extended vasodilation can occur, driving an overproduction of exudate and leading to skin maceration. Some pathologies (*e.g.* those associated with vascularity) could not produce enough exudate to supply the injury needs, such as cell migration, hindering the healing. The exudate in chronic wounds is also considered toxic for cells, slowing down the recovery. This kind of exudate has a high chance of being colonized by bacteria. For all these reasons, the exudate of chronic wounds must be assessed and treated properly to

* Corresponding author.
E-mail address: carmen.alvarez.lorenzo@usc.es (C. Alvarez-Lorenzo).
[1] These authors equally contributed to the work.

https://doi.org/10.1016/j.ijpx.2024.100288
Received 31 August 2024; Received in revised form 28 September 2024; Accepted 1 October 2024
Available online 16 October 2024

reduce the healing time (Tickle, 2016).

Dressings are the most common way to handle fluids in wounds (Minsart et al., 2022). Therefore, the way the dressing material interacts with the exudate plays an important role in wound management and resolution (Santamaria et al., 2023). Traditional wound dressings of cotton, bandages and gauzes mainly isolate the wound from contaminants, but can cause an excessive absorption of the exudate leading to dehydration or can damage the tissue by strong adhesion to the wound bed. To overcome these problems, new dressing materials have appeared in the last few years such as foams, sponges, nanofiber films and hydrogels (Sánchez-Machado et al., 2023; Zhang et al., 2024). Hydrogels are highly hydrophilic polymeric networks that can retain hundreds of times their weight in water. Therefore, using hydrogels as wound dressings may keep a moist environment while absorbing and retaining the exudate (Amante et al., 2024). The hydrogel swelling in exudate fluid can also promote proliferation and migration (Op't Veld et al., 2020; Domínguez-Robles et al., 2023). Although much less studied, the exudate itself can also have an impact on the performance of the dressing, and changes in volume and composition could strongly alter the release rate of drugs incorporated in the dressings (Agrawal and Purwar, 2018; Maver and Maver, 2023).

The World Union of Wound Healing Societies (WUWHS) defined in 2007 the concept of TIME, that involves four evaluation steps (Tissue, Inflammation/infection, Moisture balance, Edge of the wound) to carry out a systematic and individualized approach for the assessment of chronic wounds. The aim of TIME is to provide a better treatment and to decrease the healing time. The moisture balance step involves the evaluation of the exudate in terms of production rate and composition (Harries et al., 2016). Although the standardization of wound management is critical to improve the healing rate, chronic wounds are still a big concern and there are some aspects of the exudate that are not considered. One of these aspects is the exudate viscosity. As viscosity is defined by the resistance of a liquid to flow, this could be a key parameter in the interaction with dressings. As mentioned above, the exudate should penetrate the dressing at the adequate rate and at the adequate extent (Dong and Guo, 2021). The viscosity of exudates has been measured to vary widely, reaching values as large as 0.71 Pa·s (Orlov and Gefen, 2022), depending on the quantity of proteins in the exudate, the presence of bacteria and/or biofilm, deterioration of the wound bed or residual products of the dressing material (Jones, 2015). It has been reported by clinicians that the behavior, in terms of absorption, of a dressing in wounds with different viscosity is also different. This expected different performance is, however, not considered in absorption tests of dressings before their commercialization. For example, in the European Testing Standard EN 13726:2023, the absorbency of wound dressings is only tested against an ideal exudate that is far from the real situation (Forss, 2022). The standard describes the procedure to prepare the simulated body fluid by dissolving 8.298 g sodium chloride and 0.368 g of calcium chloride dihydrate for 1 L of deionized water, which has a viscosity similar to that of pure water, *i.e.* 0.001 Pa·s. Therefore, a better knowledge of how wound dressings interact with complex exudates is essential to choose the adequate dressings for each patient in the Precision Medicine context. Despite the relevance of the topic, there is still a paucity of information on the fluid management capacity of wound dressings under more realistic conditions, and only recently a comprehensive analysis on the behavior of bordered foam dressings has been published (Gefen et al., 2024).

The present work focusses on hydrogel-like dressings obtained applying recently developed Digital Light Processing (DLP) 3D printing technologies, which allow for versatile personalization of composition, external morphology, internal architecture, and incorporation of ancillary medicinal substances and drugs (Xu et al., 2021; Joshi et al., 2023; Oh et al., 2024). The dressing must have macro and/or micro porosity to effectively uptake the exudate by capillarity. Thus, the hypothesis of this work relies on the fact that the size of the wound dressing pore and the exudate viscosity regulate the exudate uptake rate. Therefore, analyzing the effects of both variables, it would also be possible to predict how fast an exudate of a given viscosity is absorbed by a specific pore size and, therefore the obtained information can be useful for the rational design of personalized dressings that can fulfil the specific wound treatment needs according to the viscosity of the exudate.

The first objective of the work was to measure the fluid uptake rate of two simulated fluids that reproduced two values of viscosities for the wound exudates. Hydrogel-based wound dressings were prepared by 3D printing of models designed to have different pore sizes but the same number of pores (Fig. 1). Once the experimental data were obtained, the next objective was to develop *in silico* models that could simulate the uptake of the exudate. Those models could perform as a prediction tool for the behavior of wound dressings in the fluid uptake. To conduct an accurate comparison between the experimental data and the *in silico* outcomes, the hydrogel dressings were prepared using a DLP 3D printer. Among the different 3D printing techniques, vat photopolymerization enables fast production of hydrogel objects, which can be suitable as dressing materials (Xu et al., 2021; Rodríguez-Pombo et al., 2022). The computer-aided design (CAD) model created for the fabrication of the 3D printed dressing was also used to perform the *in silico* simulation of the fluid uptake, serving as a pivotal parameter to compare both experimental and predicted results. To study the differences in terms of exudate absorption, three different types of hydrogels were designed, with 0%, 30% and 60% porosity. Polyethylene glycol diacrylate (PEGDA) was selected as the main component to create the porous hydrogels. PEGDA hydrogels are appropriate candidates for tissue regeneration or wound dressing due to their biocompatibility, high permeability, and intrinsic hydrophilicity to host high amounts of water, necessary for absorbing and retaining wound exudate (Browning et al., 2011). Since the pore channels of the hydrogels can distort, compared to the CAD model, after washing and freeze-drying, micro-CT images of the dressings were also taken and used for additional *in silico* simulations, showing more reliable results than when the modeling was based on the CAD model.

2. Materials and methods

2.1. Materials

Polyethylene glycol diacrylate (PEGDA, Mn 575), lithium phenyl-2,4,5-trimethylbenzoylphosphinate (LAP), and methylene blue were purchased from Sigma-Aldrich (Dorset, UK). Sodium chloride was from Labkem (Barcelona, Spain), calcium chloride dihydrate from Merck (Darmstadt, Germany) and xanthan gum (MW $>$ 1,000,000) from Acofarma (Terrasa, Barcelona, Spain).

2.2. Design of porous 3D printed hydrogels

CAD files were created using TinkerCAD (Autodesk) for the hydrogels with 0% of porosity, named as S0, and Flatt Pack (Ian Masckery, University of Nottingham) for the hydrogels with 30 and 60 % of porosity, named as S30 and S60 respectively. The selected percentage of no material was distributed in the form of pores by using the pore distribution option in Flatt Pack, that was set to be 4 $\times$ 5 along the x and y axes. The three hydrogels were designed to be 10 mm in diameter and 5 mm in height, and the pores were created in the shape of primitive honeycomb. The CAD file (.stl) was first processed and sliced using Chitubox software (China) to obtain the 2D images for the layers before uploading to the printer program. The layers had the same dimensions as the designed structure.

2.3. Photosensitive ink and 3D printing

The photosensitive resin was prepared by mixing PEGDA (35% wt) with distilled water (64.975% wt) in an amber vial and stirred until homogeneity. Then, 0.025% of LAP was added and the mixture stirred

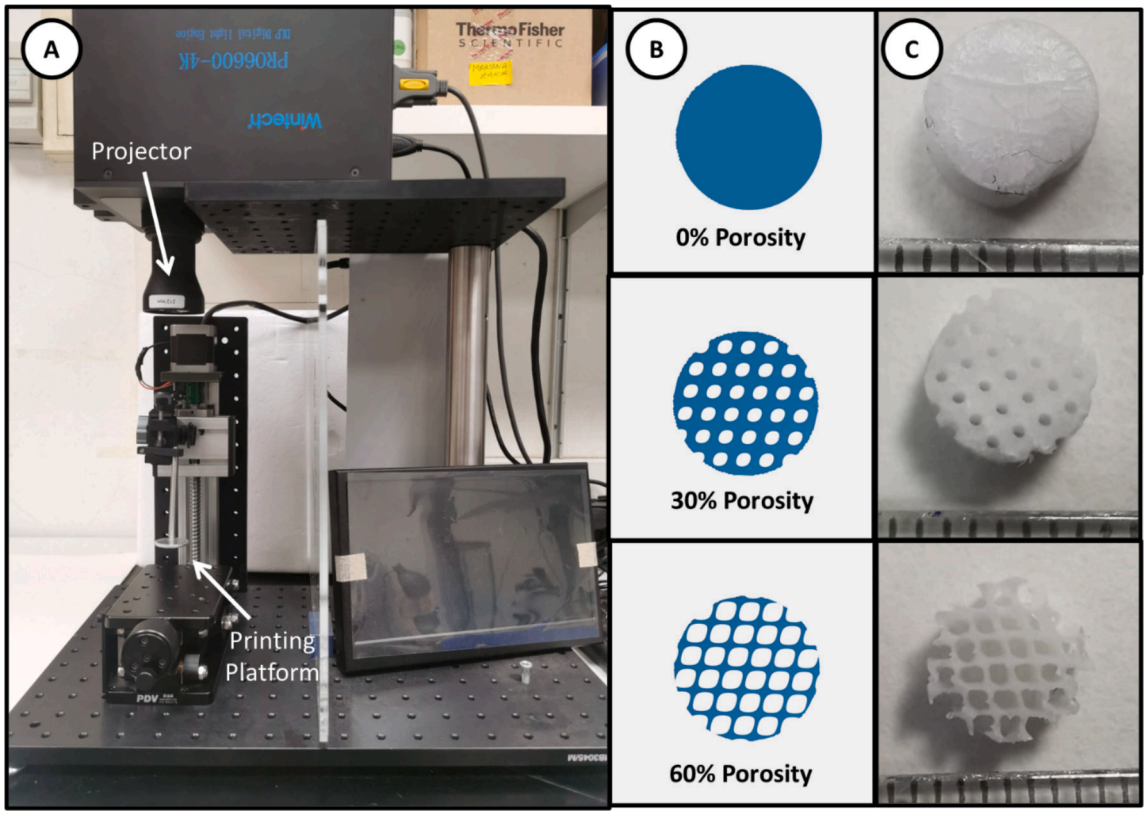

Fig. 1. (A) Top-down DLP 3D printer used for the preparation of the hydrogel dressings. (B) CAD-files of the designed hydrogels with 0%, 30% and 60% porosity, from top to bottom. (C) Appearance of the freeze-dried dressings before used (separation between tick marks represents 1 mm).

until complete dissolution.

The top-down DLP-based 3D printer consisted in a building platform that moves down into the ink container and a digital light projector (Wintech DLP6500, USA) placed on the top and facing down, composed of a digital mirror device (DMD), a UV light source (405 nm), and UV optical lenses (f = 210 mm) (Fig. 1A). First, the platform height was adjusted to the focal point of the projector (21 cm distance) to ensure the maximum resolution. Then, the platform was placed inside the resin container filled with photosensitive ink until flattened with the surface of the platform. The printer software was used to adjust the printing parameters: light intensity (10%), number of layers (1 layer) and layer height (5 mm), while the exposure time varied depending on the hydrogel and was 30, 35 and 50 s for S0, S30 and S60 respectively (Fig. 1B).

The printed hydrogels were soaked twice in ethanol and then in water for 10 min before post-curing. The post-curing method consisted of placing the hydrogel in an oven (Heraeus I42, Germany) at 4 cm of a 375 nm UV-lamp (Philips BLB F8 T5, Netherlands) 5 min per face at room temperature. Finally, the dressings were washed with 3 to 5 water changes per day until the disappearance of the typical monomer absorption bands at 190–200 nm (Agilent 8453 UV–Vis spectrophotometer, Agilent Technologies, UK). The washed dressings were frozen at −80 °C and freeze-dried before use (Fig. 1C).

2.4. Dressings physical characterization

The morphology of each dressing was studied as freeze-dried and after the exudate uptake experiments. Dressings of each composition ($n \geq 3$) were measured using a Caliper Digital Electronic (Fowler™, Newton, MA, USA). Photographs of the top view of each freeze-dried dressing were taken using a ruler as a reference (Fig. 1C).

The fluid uptake was estimated by weight using the dried mass of the dressing as m_0 and the swelled mass as m_1 measured after the experiments. The excess of liquid was blotted with filter paper before weighing. The % of fluid uptake was estimated using the following formula:

$$\%Fluid\ uptake = \frac{m_1 - m_0}{m_0} x100 \quad (1)$$

The same equation was used to estimate the changes in size (diameter and height) by using initial and final measures instead of m_0 and m_1.

Surface topography was examined using field emission scanning electron microscopy (FESEM Ultra Plus, Zeiss, Oberkochen, Germany). Freeze-dried dressings were placed on metal supports and sputter-coated with 10 nm thick gold film (model Q150T-S, Quorum Technologies, Lewes, UK) before viewing. Some dressings were cut with surgical blades to obtain cross-sectional views.

Models of the freeze-dried hydrogels and the corresponding swollen hydrogels were created using high-resolution microcomputed tomography (micro-CT) scanner (Skyscan 1272, Bruker, Kontich, Belgium). Images were obtained by scanning at 10 μm/pixel with a resolution of 2016 × 1344, exposure of 200 ms and voltage, current and rotation step setting of 50 kV, 200 μA and 0.4°, respectively. Reconstruction of the 3D structure was carried out using the software NRecon (Bruker-microCT) and then, a 3D model (.stl) was obtained using the software CTAn (Bruker-microCT). To carry out the scanning of the swollen hydrogels, the freeze-dried dressings were immersed for 5 min in a 1:10 dilution of OmnipaqueTM (GE Healthcare) staining solution and then blotted superficially with filter paper.

2.5. Simulated exudate fluid (SEF) preparation

A saline solution used as a control test solution in dressing performance was prepared by dissolving 8.298 g of NaCl and 0.368 g $CaCl_2{\cdot}2H_2O$ in 1 L of water (Davies, 2012; Forss, 2022). Xantham gum was added to this solution to simulate different viscosities of the

exudate. The dispersion was kept under mechanical stirring using paddles (VWR VOS 60 control, VWR) for 1 h at 600 rpm and then at 400 rpm overnight. Finally, the SEF was autoclaved at 121 °C for 20 min. The solution was kept at 4 °C for 1 week and warmed at RT before use. The pH of the prepared SEF was determined using a pH-meter Crison GLP22 (Barcelona, Spain). Aliquots of 200 mL for each SEF were taken out and a spatula tip of methylene blue was added to stain the solution.

The viscosity of the SEF was determined in a Rheolyst AR-1000 N rheometer equipped with an AR2500 data analyzer, a Peltier plate and a steel cone geometry (60 mm, 2.1°) (TA Instruments, Newcastle, UK). The experiments were carried out at 20 °C applying a continuous shear rate ramp from 0.05 to 200 s^{-1}. The viscosity (η) *versus* shear rate ($\dot{\gamma}$) plots were analyzed using the Power law model.

$$\eta = m \cdot \dot{\gamma}^{n-1} \quad (2)$$

In this equation, m is the consistency index, *i.e.* the viscosity at 1 s^{-1}, and n is the Power law index or fluidity index, which ranges from 1 for Newtonian fluids to 0 for very shear-thinning (pseudoplastic) fluids (Xuewu et al., 1996). Values of n above 1 are indicative of shear-thickening (dilatant) fluids.

The surface tension of the SEF was estimated using a tensiometer Lauda Scientific TD1 (Lauda Scientific, Germany) fitted with a Platinum ring.

2.6. SEF absorption experimental measurement

The vertical absorption of SEF through the pores of each dressing was monitored using a video set-up that consisted of a porous sintered filter plate from a Buchner glass funnel placed in a glass Petri dish and a PixeLINK (Canada) scientific camera with an optical lens (f = 35 mm) at the focal distance from the filter with a slight elevation and inclination (Fig. S1). The dressings were firstly pre-wet in SEF solution (colorless) and blotted with paper to eliminate the excess of liquid in the macropores. Then, the dressing was placed on the surface of the filter plate, which had previously been wet in a blue-stained SEF solution and placed in a Petri dish filled with the stained SEF solution until half the height of the filter plate. The videos were recorded using the PixeLINK software and subsequently analyzed using the open-source program Tracker (Open-source physics) (Videos S1-S4 in Supplementary Material). The program took the height of the dressing as a reference and then the movement of the stained SEF was monitored frame by frame with a pixel tracking. Staining the exudate solution facilitated the tracking of the fluid along the pore. The experiments were carried out in triplicate for each type of dressing and for the two SEFs prepared with different contents in xanthan gum.

2.7. SEF absorption simulation

The *in silico* study of the exudate uptake for the dressing was developed using the software StarCCM+ (Siemens Industries Digital Software, Simcenter STAR-CCM+, v 2302, Siemens 2023) based on computational fluid dynamics (CFD). This software uses protocols that allow dividing the region of study into smaller parts at which Navier-Stokes equations are numerically solved. The software offers a highly configurable environment in which a wide variety of setups is possible with enough trial and error. StarCCM+ also includes methods to generate a custom mesh for the problem at stake; several meshes have been tried to find an intermediate point between fast and accurate simulations.

Since the focus of this study was the behavior of different viscosity liquids when in contact with the proposed hydrogel dressings, the simulations revolved around the multiphase interaction and volume of fluid (VOF) modules. These modules enabled the simulation of a region with a mixture of substances in different states of matter, in our case gas and liquid.

The capillarity effect is mainly given by the angle of contact between the chosen viscous liquid and any of the surfaces on the model. These angles were set independently for each solid surface and were how we specified the type of solid material we were working with. To avoid interferences due to the irregular surface channels of the 3D models created from the printed hydrogels, the 3D mesh resolution was increased keeping the other simulation conditions the same. The increment in the mesh resolution was done to obtain a higher precision of the solvent front position, increasing, therefore, computational resources.

3. Results and discussion

3.1. Design and characterization of the dressings

All the dressings were designed in a cylindrical form of 10 mm diameter and 5 mm height (Fig. 1). The shape and the number of pores distributed along the hydrogel were set to be the same for both types, namely the only difference between 30 and 60% of porosity is the size of the pore (Fig. 1B and C).

PEGDA-based polymers are receiving increasing attention as components of hydrogel dressings due to their intrinsic hydrophilicity and capacity to retain water molecules. PEGDA and LAP are also frequently used together, for example in water solutions of 25% PEGDA and 0.5% LAP (among other acrylates/crosslinkers) (Lan et al., 2023). A water-based ink composition of solely PEGDA and water was chosen to avoid any changes in the hydrophilicity of the polymer chains triggered by the presence of other components. Also, the minimum quantity of LAP in the ink that allowed good printability was used to preserve the green chemistry and sustainability principles. The ink composition that provided high 3D printing fidelity and relatively fast production of hydrogels was 35% of PEGDA with 0.025% of LAP in water.

The 3D printed hydrogels were washed and post-cured under UV-light to ensure complete removal of unreacted monomers. The freeze-dried dressings had a sponge-like consistency, white color, and visible regular porosity according to the CAD design (Fig. 1C). Height and diameter were, however, slightly smaller than in the CAD model (Table 1), which could be attributed to a contraction of the hydrogel network during the freeze-drying process and/or a scalation of the DLP during the layer projection. Porous dressings are commonly supplied in a dry state to reduce the weight of the packaging and increase the stability against microbial growth. These reasons motivated the study after drying of the hydrogels, but depending on the application moist hydrogels (solely or pre-loaded with an ancillary medicinal substance) could also be used directly.

Surface and porosity were evaluated using SEM micrographs, which showed smooth surfaces for the three kinds of hydrogels (Fig. 2). Interestingly, the micrographs revealed unidirectional straight lines alongside the material, which were more evident in higher magnifications. This pattern presented in the surface could be attributed to the DMD pattern of the projector.

Table 1
Average weight, diameter (d) and height (h) for the freeze-dried dressings, and the size of their pores according to the CAD design and obtained from SEM images after freeze-drying and after re-swelling ($n = 6$).

Hydrogel	Mass (mg)	d (mm)	h (mm)	CAD pore size (μm)	SEM pore size (dried) (μm)	SEM pore size (wet) (μm)
S0	105.0 ± 6.0	6.32 ± 0.09	3.45 ± 0.15	0	0	0
S30	99.6 ± 8.9	6.28 ± 0.26	3.66 ± 0.09	963.9 ± 14.1	393.7 ± 26.7	650.7 ± 81.9
S60	32.4 ± 2.7	5.36 ± 0.38	3.61 ± 0.21	1331.2 ± 14.2	1097.3 ± 25.8	1280.6 ± 37.1

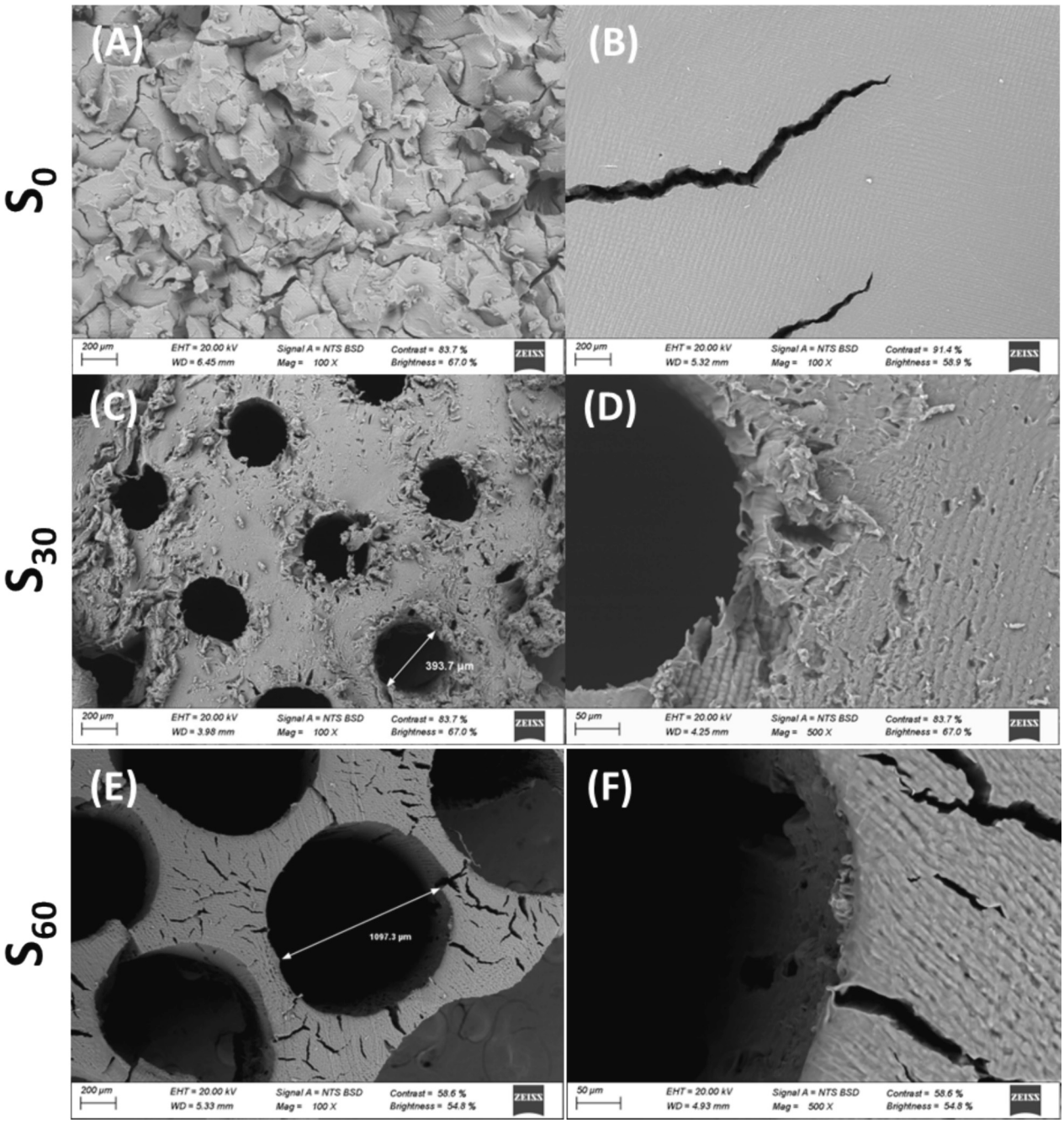

Fig. 2. (A,B) Cross-section and surface images at 100× of freeze-dried S0 dressing (scale bar 200 µm); (C,D) Cross-section images of freeze-dried S30 dressing recorded at 100× (scale bar 200 µm) and 500× (scale bar 50 µm); and (E, F) Surface images of freeze-dried S60 dressing at 100× (scale bar 200 µm) and 500× (scale bar 50 µm), respectively.

Pore size of dried S30 and S60 hydrogels was also assessed through SEM images using the image processing software ImageJ (LOCI, University of Wisconsin). For each hydrogel, the average pore size (4 measurements of the diameter in different pores) was obtained and compared with the size of the CAD model (Table 1). The hydrogel size and pore size decreased after freeze-drying approx. 30% for S60 and 60% for S30 compared with the STL model of 10 × 5 mm (diameter x height). Once re-swollen S60 hydrogels recovered approx. 99% the initial pore size, while in the case of S30 hydrogels the pore size remained below 70% initial values.

3.2. Simulated exudate fluid (SEF)

The behavior of the hydrogels regarding fluid uptake was investigated using two exudate-substitute fluids (SEFs) prepared with standard saline solution (containing NaCl and $CaCl_2$) to which different proportions of xanthan gum were added to modulate their viscosity. Studies on full-thickness wounds reported very varied exudate volume per day, ranging from 0.0 to 47.0 mL/day with a mean value of 6.0 mL/day (Iizaka et al., 2011). Also, different viscosity values have been reported. For example, the viscosity of human plasma from fresh blood has been estimated to be 1.7 times greater than that of water with values ranging from 1.35 to 1.25 mPa·s (Malomuzh et al., 2020); the lowest values corresponding to diabetic patients (Mellinghoff et al., 1996). Other

studies have described exudate viscosity values as high as 230 to 710 mPa.s (Orlov and Gefen, 2022). Thus, to cover a biorelevant range of viscosity values, two SEFs were prepared containing 0.1% and 0.2% (wt) of xanthan gum as thickening agents. The dispersions were vigorously stirred and then autoclaved. After one week kept at 2–8 °C, the SEFs were warmed up, and the dynamic viscosity (Fig. 3), surface tension and pH were estimated (Table S1).

The 0.1 % xanthan gum solution provided an increment in the viscosity compared to water of up to 26.5 mPa·(*vs.* 1 mPa·s), while the dynamic viscosity (consistency index) of 0.2% xanthan gum solution was one order of magnitude larger (Table S1). In addition, the surface tension of the SEF solutions decreased to 61.7 and 62 mN/m (0.1 and 0.2% xanthan gum, respectively) from 75.1 mN/m of water.

3.3. SEF absorption experimental measurement

The next step was to study how SEFs of different viscosities were absorbed through dressings with different pore sizes. Some parameters were controlled to minimize possible interferences. First, hydrogel macroporosity was designed to be only vertical and the dressing was exposed to the fluid from only one side of the pores, mimicking the placement on the top of the wound. Second, the freeze-dried hydrogels were first wetted in the correspondent colorless SEF to recover the initial pore size. Once rehydrated, the hydrogels were blotted gently with filter paper to absorb the excess of fluid inside the pores. This overall procedure was chosen to avoid changes in the size of the pores due to a volume phase transition while measuring fluid uptake rates.

The hydrogels rehydrated in the colorless SEF solutions were weighed and measured, and the changes in the swelling and water uptake were estimated using Eq. (1) (Fig. 3). The height of the hydrogels after rehydration was similar to that of the designed model, but the diameter values were slightly smaller. As mentioned, this could be attributed to the scalation of the model when is projected to print, which affected only the x and y axis. On the contrary, the height depended only on the axial movement of the platform and was closer to the CAD model when rehydrated. Total water uptake and swelling were similar for both types of hydrogels.

Movement of stained SEF through the rehydrated hydrogels ($n = 3$) was recorded by monitoring the position of the front of the stained (bluish) SEF (representative Videos S1 to S4 in Supplementary Material) and further analyzed with the video analyzer program Tracker. PEGDA-based hydrogels have the unique advantage of being completely transparent when hydrated, which allow visualizing the wound bed directly through the dressing without removing it. Hydrogels placed on the filter plate impregnated with the stained solution evidenced a rapid change in color (from colorless to bluish) from the bottom to the top, meaning that SEF uptake occurred very rapidly (Fig. S2). The quantification of the time it takes for the fluid to reach the top of the hydrogel was done using the tracking option of the software, and it was possible to manually select the front of the fluid using a frame-by-frame transition. Since the hydrogel was blotted before been placed in the set-up, the vertical fluid uptake through the pores was visualized due to the stained solution as a blue straight line or, in other cases, as a wider colored front of absorption color (Fig. 4). In some cases, the position of the fluid front was tracked and positioned along the channel at the selected video frames by using the height of the corresponding rehydrated hydrogel as a reference.

The dressing with no porosity (S0) were discarded due to the excessively long uptake times. Also, the SEM images did not evidence measurable porosity, and thus simulation of the fluid absorption was not possible for S0. Analysis of the videos evidenced that the fluid sorption was not homogeneous when compared among pores of the same

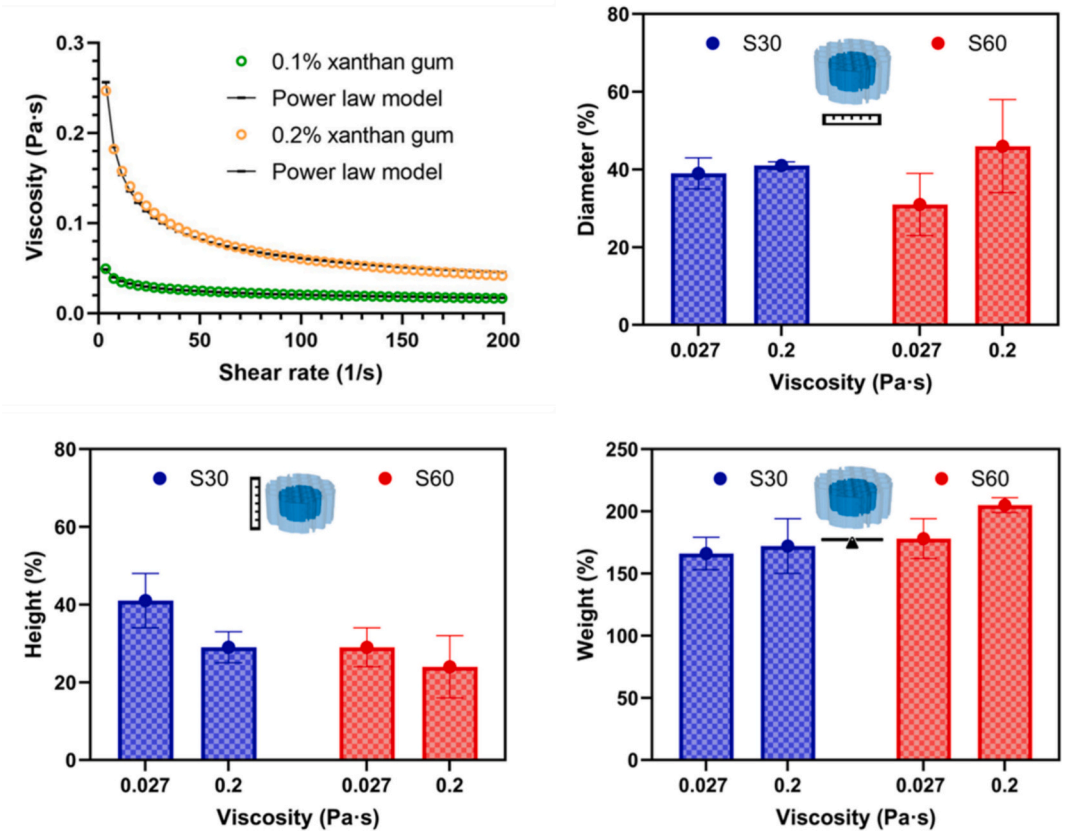

Fig. 3. Viscosity of the SEFs prepared with 0.1% (green) and 0.2% (yellow) of xanthan gum at 20 °C (circles) and the correspondent power law fitting model (lines). Bar graphs represent the increment in the size (diameter and height) and the water uptake (weight) when the freeze-dried hydrogels were rehydrated in SEFs of low (0.027 Pa·s) and high (0.2 Pa·s) viscosity. (For interpretation of the references to color in this figure legend, the reader is referred to the web version of this article.)

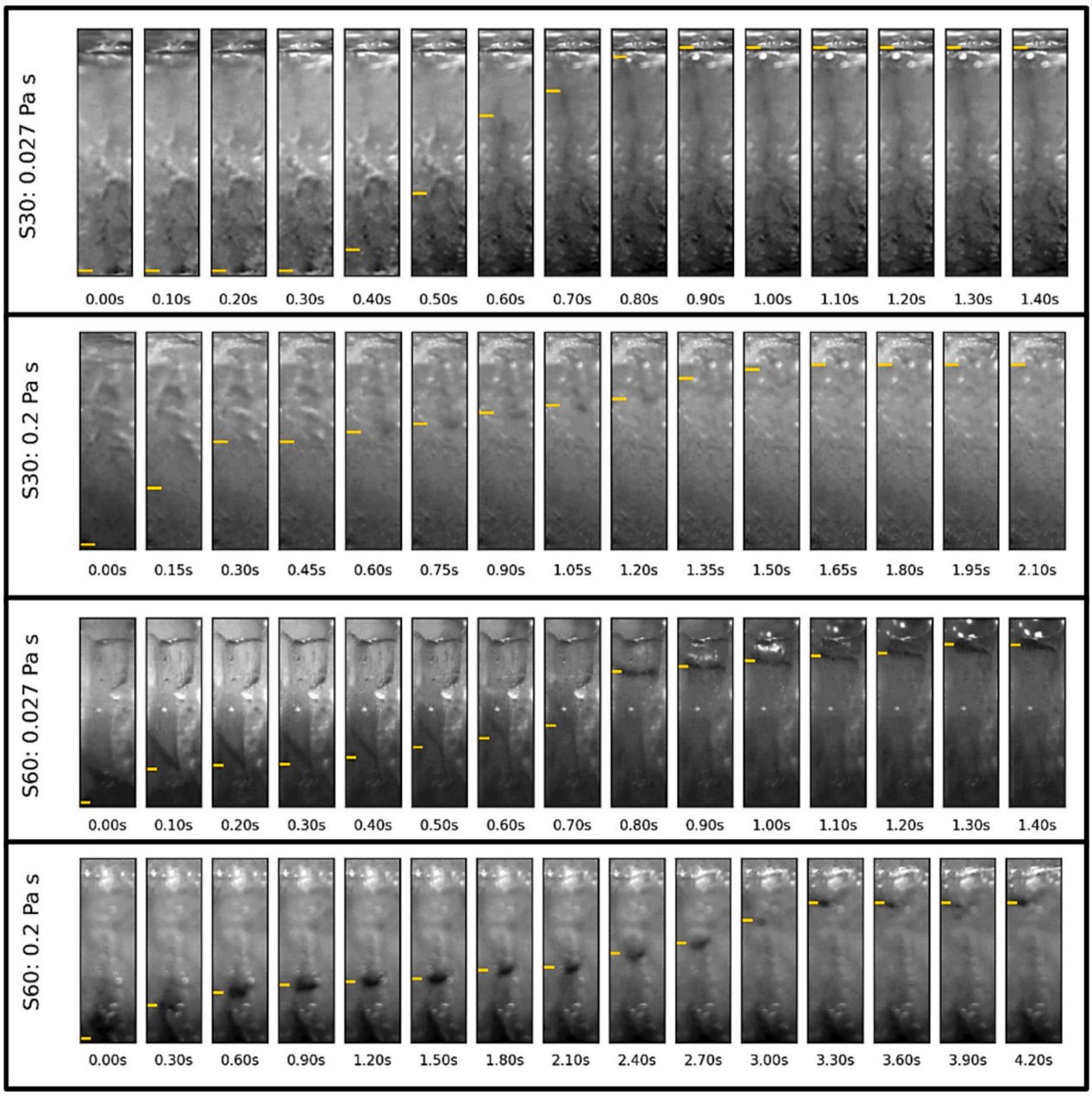

Fig. 4. Video frames of the SEF uptake along one pore of each hydrogel. The front of the liquid is marked with a yellow line. (For interpretation of the references to color in this figure legend, the reader is referred to the web version of this article.)

hydrogel. Some of the uptakes started immediately after the hydrogel touched the setup platform, but others were delayed by a few seconds. In almost all recordings, the end of the tracking was easy to set because the stained solution reached the top of the pores. The tracking of the fluid along the pore channel could only be done from the pores that were situated in front of the camera thanks to the colorless/transparency of the dressing. However, the tracking was not a straightforward task, although the color change was evident, in some cases, the front of the fluid was hidden with the color changes of the surroundings. Regardless of these inconveniences, fluid sorption through several pores was tracked. Three different methods were applied to collect the data, as follows.

1) First method: the instant when the hydrogel touched the wet filter disc was selected as the zero time, and the uptake was visually followed until the fluid reached the top of the hydrogel defined as final time. The absorption rate was estimated by the corresponding height of the hydrogel divided by the difference between the selected time points.
2) Second method: the instant when the front of the solvent started to ascend was selected as the zero time, and the uptake was visually followed until the fluid reached the top of the hydrogel defined as final time. The absorption rate was estimated by the corresponding height of the hydrogel divided by the difference between the selected time points.
3) Third method: the upward movement of the fluid through the channels was tracked by selecting the front of the fluid at different time points by frame-by-frame transitions.

To compare the outcomes from methods 1 and 2, the velocities obtained were transformed in the time that the fluid took to ascend 5 mm (theoretical height of the hydrogel). Both methods revealed similar

average times when the correspondent mean values were compared; however, the standard deviations for method 2 were smaller than for method 1 (Fig. 5A and B). Therefore, method 2 was chosen to obtain the time the SEF needs to cross the hydrogel.

The visualization and data curation suggested that for S30 hydrogel the absorption rates were determined by the viscosity of the fluid. The time predicted for the fluid to ascend 5 mm in S30 was 0.78 ± 0.37 s for SEF of 0.027 Pa·s and 2.61 ± 0.59 s for SEF of 0.2 Pa·s. The lower absorption rate as the exudate viscosity increases is consistent with results from previous studies carried out with different dressing (Forss, 2022).

The data processed for S60 hydrogel recordings suggested that the uptake pattern was similar to that of S30 hydrogels, namely the higher the viscosity the longer the time to reach the top. While the SEF of the lower viscosity needed 2.18 ± 0.70 s to reach the top, the SEF with higher viscosity took 5.36 ± 3.01 s. However, recordings of S60 hydrogels (especially those in contact with the fluid of 0.2 Pa·s) evidenced larger data dispersion (Fig. 5B), which could be attributed to the strands of this pore size. The only difference between S30 and S60 hydrogels is the size of the pore, which in turn means that strands ("lateral walls") between pores are, therefore, thinner in S60 than in S30. Thus, the lateral walls of S60 pores may be prone to be distorted during swelling and blotting. Distortions of the strands may alter the pore diameter and shape providing different uptake rates. Also, SEM images evidenced some fractures in those strands, so that the pores with some cracks could act as a larger pore, and hence, varying the absorption rate. Despite these uncertainties, the uptake was overall faster for the hydrogels with lower pore size (S30 *vs.* S60), evidencing the effect of capillary forces, which inversely correlate with the diameter of the pores according to the Young-Laplace equation (Tuller and Or, 2005).

The third method was chosen to visualize how the fluid was positioned along the height of the pore and to study variations in the rates along the upward movement. For this method, only the pores closer to the camera were recorded and the position of the fluid tracked. The fluid position data was first normalized by using the final height of the tracking as 100%, namely the percentage of pore filled with fluid, and represented as a function of time (Fig. 5C and D). The data representation suggested that the rates (or the slope between two consecutive points) were faster at the beginning and slowed down with the height. The experiments using the low viscosity SEF exhibited faster rates for S30 than S60 hydrogels, which is consistent with other methods. The experiments with the high viscosity SEF did not evidence correlation between the pore size and the absorption. The decrease in absorption rate as a function of the height is explained by the fact that the attractive interaction between the hydrogel and the SEF, which causes the liquid to rise to the top of the channel, is counteracted by the gravitational force on the liquid column, which contribution becomes more relevant as the diameter of the pore increases (Ramsden, 2016).

3.4. SEF absorption simulation

The CAD models created for 3D printing were used in the CFD software to simulate the interaction of the hydrogels (pore size) with the two SEFs differing in viscosity. To predict the behavior, the 3D models were encapsulated in the software in a cylindrical volume slightly larger than the model. The used cylinder was 18 mm tall and, initially, the volume was only filled with the viscous liquid at the first 3 mm from its base; the rest of the volume was filled with air. Inside this cylinder, a virtual hydrogel was placed high enough, so the base of the hydrogel was barely touching the surface of the liquid. The contact angle between the liquid and the cylinder was set to 90° to minimize interferences; for the hydrogel wall this value was set to 25°.

Simulations with different viscosities were made from $8{\cdot}10^{-4}$ Pa·s (water) to 0.7 Pa s, *i.e.* the maximum exudate viscosity according to reported data (Orlov and Gefen, 2022). Both S30 and S60 hydrogels

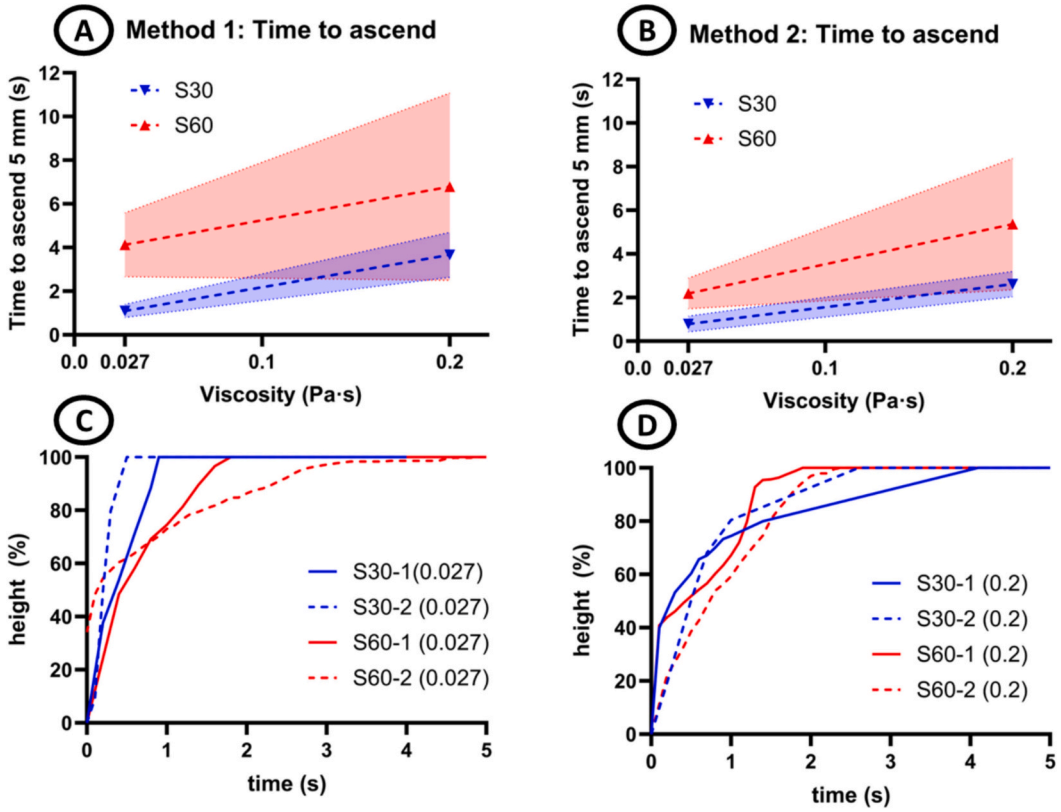

Fig. 5. (A, B) Results obtained by analyzing the SEF uptake through S30 (blue line) and S60 (red line) hydrogels, applying methods 1 and 2. Triangles represent the mean time that the SEF needs to ascend 5 mm (pore height) for each viscosity. Standard deviations are represented as shaded colors. (C, D) Position of the solvent at a certain time of the experiment for low- and high-viscosity SEF, respectively. Two replicates were represented for each type.

were used for the model. To measure the simulated liquid level, the percentage of liquid at several points in a vertical line was sampled over time. When the liquid-gas mixture in the pores reached a concentration of 70% (or volume fraction) of liquid or higher at any point we assumed that the full height of the hydrogel was filled with the liquid; this methodology was named as simulation 1. The measurement of the liquid level was also repeated but sampled when the liquid reached a concentration of 99% or higher, this methodology was named as simulation 2 (Fig. 6).

Simulations 1 and 2 evidenced that the time to fill the pore was determined by the viscosity of the fluid, where the more viscous fluid took longer times to escalate through the pore channel model. This is consistent with other CFD numerical simulations (Andredaki et al., 2020; Neunkirchen et al., 2022) that reported that droplets of liquids with higher viscosities took longer time to penetrate through a column of specific porosity. Simulation 1 suggested that the pore size could regulate the time that the fluid reached the top of the hydrogel as can be seen in Fig. 7B, where the liquid reached the top faster for the smaller pore size. However, in simulation 2 the pore filling seemed to be independent of the pore size (Fig. 7C). Interestingly, when Fig. 7C was zoomed in (Fig. 7D and E), the difference between pore sizes were in terms of milliseconds and were faster for the largest pore size.

3.5. *In vitro and in silico comparison*

Attending only to the fluid viscosity, for both *in silico* and *in vitro*, the upward movement of the fluid through the pore was apparently dependent on the viscosity, where absorption times were higher for the SEF of 0.2 Pa·s. Regarding the pore size, in simulation 1, when the front of the fluid was considered the 70% of the volume fraction, the difference in time between hydrogels with different pore size in the same fluid were roughly 50% longer for S60 than for S30 (Table S2), suggesting that the pore size also contributed to the uptake rate. *Per contra*, when the volume fraction was considered 99% (simulation 2) the fluid

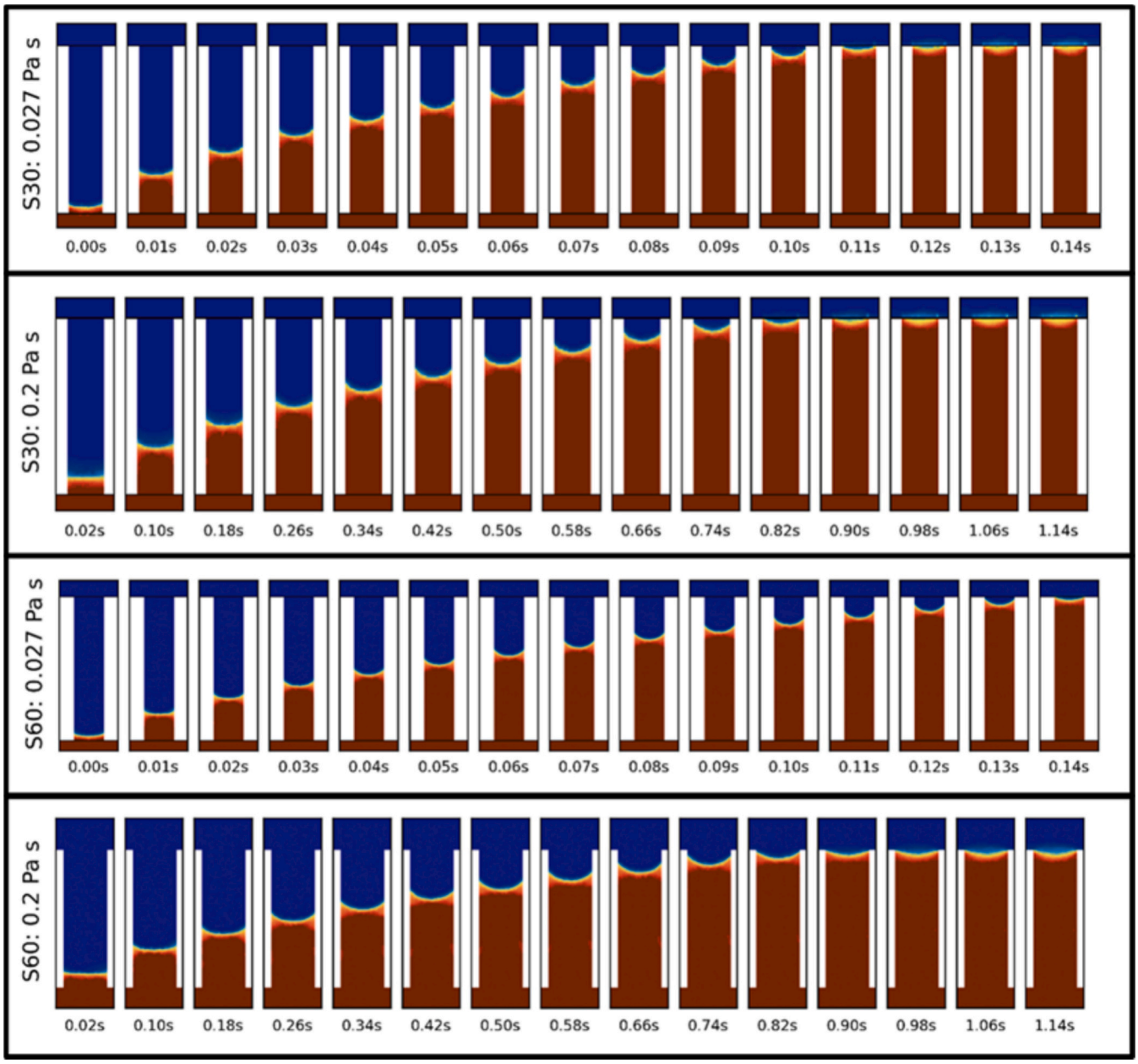

Fig. 6. Evolution of one single pore filling using simulation method 2 for each hydrogel in the low and high viscosity SEFs. Brown color represents volume fraction of exudate while blue represents air. (For interpretation of the references to color in this figure legend, the reader is referred to the web version of this article.)

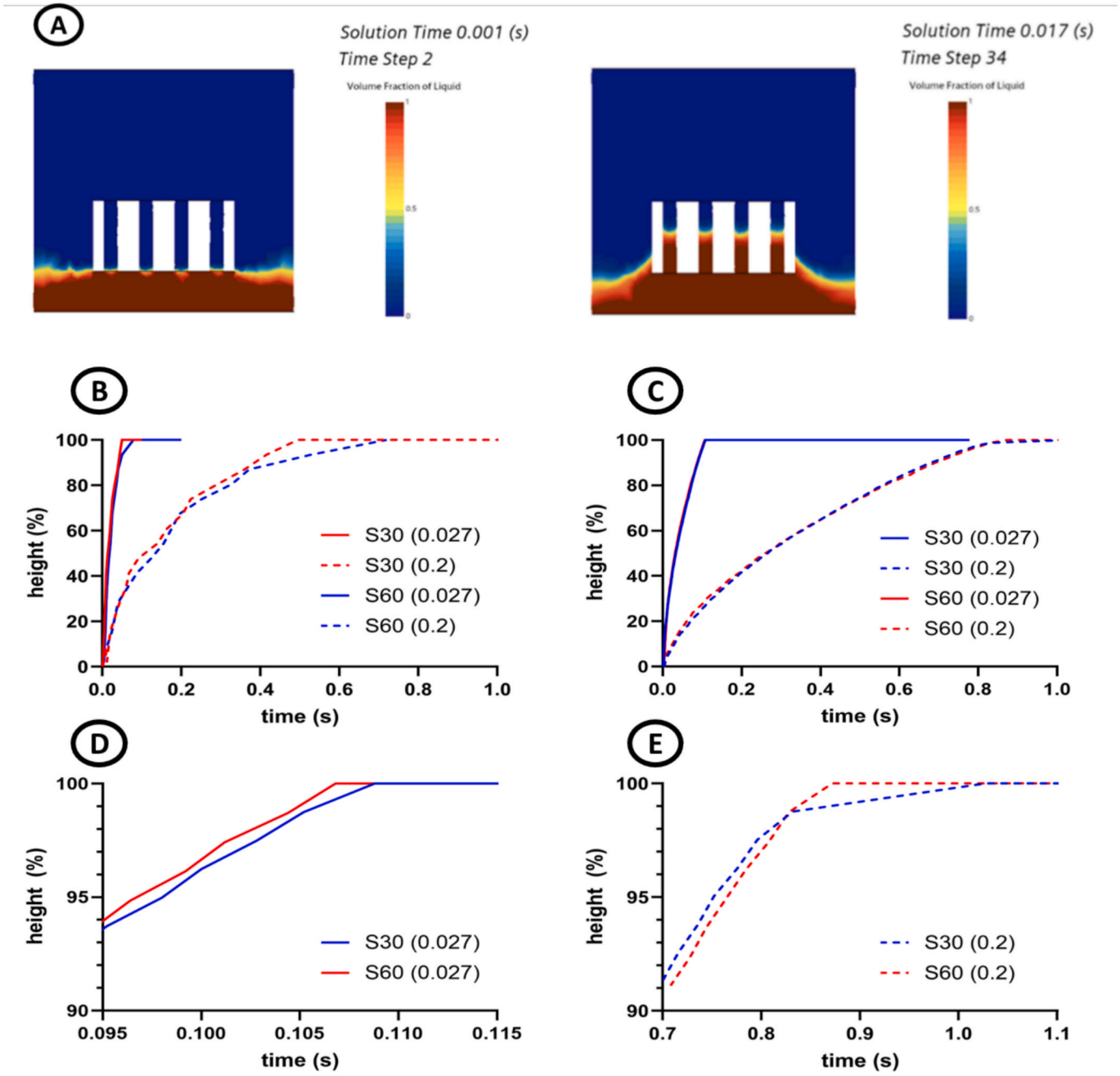

Fig. 7. (A) Examples of frames for the video of the uptake simulation generated using the CFD software. Simulation corresponded to the S30 hydrogel in a fluid of viscosity 0.02 Pa·s. The hydrogel model was represented in white color and the image corresponded to a vertical interior section of the hydrogel to see how the liquid was absorbed through the pores. The volume fraction of liquid was represented in the right bar as 0% (blue) and 100% (dark red). (B, C) Percentage of pore filled by the fluid (%) at certain time points from simulation 1 and 2, respectively. (D, E) Amplifications of simulation 2 from the final time points of low and high viscosity SEFs, respectively. (For interpretation of the references to color in this figure legend, the reader is referred to the web version of this article.)

reached slightly faster the top of S60 than S30 hydrogel. *In vitro* experiments suggested that for the lower viscosity SEF, the pore size may influence the uptake rates. However, the experiments with high viscosity SEF did not evidence a clear influence of pore size, while the average time obtained with methods 1 and 2 was longer for S60 than S30, the times obtained by tracking the fluid using method 3 were shorter.

Methods 1 and 2 of data collection displayed the experimental time that the fluid took to fill the entire pore channel. The comparison of the experimental data with the corresponding simulation time evidenced that both follow similar trends, but simulations with fluids of any viscosity rendered faster filling of the pores. This could be explained as the simulation did not consider the fluid uptake intrinsic to the material, just the movement through the architectural vertical pores due to capillarity. Also, the simulations using CAD models considered the hydrogel pores as regular along all the structure, which was not the experimental situation as seen in SEM. So that, when the hydrogels were tested *in vitro*, the fluid that was absorbed by the polymeric material among pores, and distortions or structural breakages along the channels could slow down the absorption rates through the pores. Interestingly, tracking the position of the SEF front along the experiment, it was noticeable that the behavior of the liquids during the upward movement was quite similar to the simulated ones; the movement being faster at the beginning of the uptake and slowing down near the top.

The effect of lateral fluid absorption (spread within the material of the wall of the pores) was modeled by Neunkirchen et al. (2022) using a tube model with porous walls. The simulation of the fluid filling suggested that the uptake rate through the capillary was slowed down due to the fluid escaping from the lateral pores, and the model outcomes were also corroborated experimentally with different materials. This situation may be similar to the experimental behavior of S30 and S60 hydrogels where the microporosity of the material and its hydrophilicity could act as an external force that drains the liquid horizontally, slowing down the vertical absorption rates.

The distortion of the structure and its correlation with the absorption rates were evaluated by micro-CT scanning of the freeze-dried and re-swollen hydrogels and reconstructing the 3D model (.stl). The CFD simulations using CAD models provided an ideal uptake rate considering all the pores equal in terms of surface regularity. However, during the post-printing process, the hydrogels experienced volume shrinkage when freeze-dried and then a volume transition when swelled again to recover totally or partially the initial volume (data in Table 1). So that the structure could be compromised during the experiments, as observed in SEM analysis. It was evident that a more realistic 3D model approximation is necessary to better understanding the behavior of the dressings when they are in contact with the wound exudate. To tackle these differences a 3D model of the post-processed scaffolds was created by the reconstruction of the scanned images obtained by micro-CT analysis.

3D models of the freeze-dried and swollen hydrogels were obtained (Fig. S3), and the simulation was carried out again for S30 hydrogels using these models. The volume shrinkage was evident when compared both printed models, freeze-dried and swollen, and also the distortion of the pore strains. Simulation using the micro-CT model of the swollen S30 hydrogel (Fig. S3B) in the SEF of 0.027 Pa·s displayed two interesting outcomes. First, the simulation provided different uptake times for each pore (Fig. S4) which was more consistent with the *in vitro* results where the recordings confirmed the variability in terms of absorption times for each single pore. Second, the absorption times obtained in the simulation using the real micro-CT information were longer than those obtained using the ideal CAD model. While for simulation 1 and 2 the predicted times were 0.05 s and 0.109 s respectively, the micro-CT based simulation showed a mean value of 0.21 ± 0.02 s (Fig. 8) which was closer to the correspondent experimental value of 0.78 ± 0.37 s.

Although simulations of the 3D printed hydrogels did not provide the same absorption times as the *in vitro* tests, results from the *in silico* modeling suggested that strand distortion due to handling, post processing or even swelling-deswelling may notably contribute to the variability of exudate sorption rate among pores and also to slow down the uptake. Moreover, in good agreement with recent reports on bordered foam dressings, an increase in viscosity slows down the exudate flow rate (Gefen et al., 2024) although a complex relationship with pore size can be inferred.

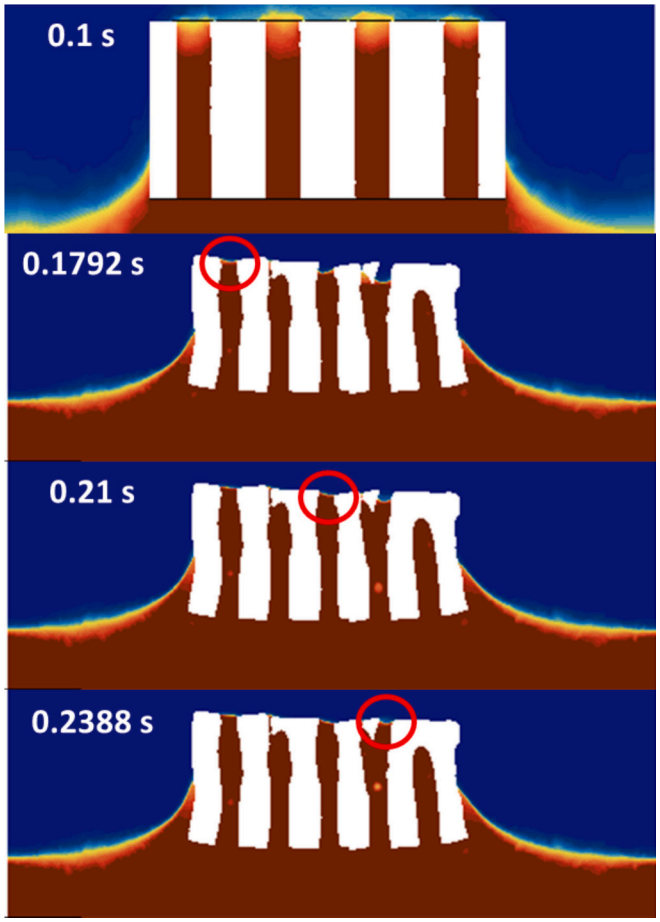

Fig. 8. Frames of the simulations when the pore was filled with the low-viscosity exudate (0.027 Pa·s). The top frame corresponds with the simulation carried out with the S30 CAD mode. Successive frames below correspond with the simulation carried out using the micro-CT model of the swollen S30 hydrogel.

4. Conclusions

Porous hydrogel networks are gaining increasing attention as wound dressings due to their intrinsic affinity for water, which allows regulating the moisture balance of wounds but also the release of a variety of ancillary medicinal substances. The fact that most hydrogels are transparent and colorless was exploited here for direct monitoring of fluid absorption and replenishment within hydrogel dressings of different pore sizes. DLP 3D printing was used to prepare dressings with very precise control of the number and allocation of unidirectional pore channels with diameters in the micrometer scale. Using two fluids that simulated one of the most frequent viscosities of exudates (0.027 Pa·s) and one of the largest viscosity conditions (0.2 Pa·s), both experimental data and computational modeling evidenced that the absorption occurs faster for low-viscosity exudates through hydrogels with smaller pores, as both factors facilitate capillary forces. Although for hydrogels with larger pores and in contact with high viscosity exudates the absorption is still quite fast, the results show large variability and are less predictable. Thus, an increase in the hydrogel pores beyond 400 μm may not facilitate exudate absorption, while it may compromise the consistency (strength) of the hydrogel dressing. Relevantly, the upward movement of exudate through the hydrogel is faster in the first few millimeters in contact with the wound bed and then slows down. This finding also draws attention to the thickness of the dressing, as thick hydrogels may make the removal of wound exudate slower.

The comparison of *in vitro* absorption and *in silico* simulation clearly highlights two relevant limitations of computational modeling, which also have a practical impact: i) spongy hydrogel dressings can be internally distorted during processing and handling, which alters the cylindrical pores compared to the CAD model used for 3D printing, and therefore, such distortions need to be considered for more accurate simulations. In parallel, spongy dressings need to be accompanied by detailed instructions for use regarding the pressure to be exerted on their structure during handling and wearing, as it can distort the pores and compromise the exudate absorption rate; and ii) the bulk of the hydrogels has an inherent affinity for water and such exudate absorption by the bulk of the hydrogel can act as a force that drains liquid horizontally, slowing down vertical absorption rates. The relevance of this last factor will depend on the hydrophilicity of the polymer network. A deeper understanding of exudate absorption may be useful for the rational design of wound dressings that regulate exudate absorption and also deliver drugs at the adequate rate for each patient.

Supplementary data to this article can be found online at https://doi.

org/10.1016/j.ijpx.2024.100288.

Funding

The work was supported by MCIN/AEI/10.13039/501100011033 [PID 2020-113881RB-I00 to C.A.L. and A.C., and PID2022-138322OB-100 to A.P.M.], Spain, Xunta de Galicia [ED431C 2024/09 to C.A.L. and A.C., and 2021-PG036 to A.P.M], and FEDER "ERDF A way of making Europe".

CRediT authorship contribution statement

Alejandro Seijo-Rabina: Writing – review & editing, Writing – original draft, Visualization, Validation, Software, Methodology, Investigation, Formal analysis, Data curation, Conceptualization. **Santiago Paramés-Estevez:** Writing – review & editing, Writing – original draft, Visualization, Validation, Software, Methodology, Investigation, Formal analysis, Data curation, Conceptualization. **Angel Concheiro:** Writing – review & editing, Supervision, Resources, Project administration, Funding acquisition, Conceptualization. **Alberto Pérez-Muñuzuri:** Writing – review & editing, Visualization, Software, Resources, Funding acquisition, Formal analysis, Conceptualization. **Carmen Alvarez-Lorenzo:** Writing – review & editing, Writing – original draft, Visualization, Supervision, Resources, Project administration, Methodology, Funding acquisition, Formal analysis, Data curation, Conceptualization.

Declaration of competing interest

The authors declare that they have no known competing financial interests or personal relationships that could have appeared to influence the work reported in this paper.

Data availability

The data that supports the findings of this study are available in the supplementary material of this article.

Acknowledgements

Luis Diaz-Gomez from University of Santiago de Compostela is acknowledged for his assistance with micro-CT studies. A.S-R. acknowledges a PRE2021-098268 fellowship financed by MCIN/AEI/ 10.13039/501100011033 and FSE+.

References

Agrawal, A., Purwar, R., 2018. Swelling and drug release kinetics of composite wound dressing. Indian J. Fiber Text. Res. 43, 104–111.
Amante, C., Neagu, M., Falcone, G., Russo, P., Aquino, R.P., Nicolais, L., Del Gaudio, P., 2024. Hyaluronate loaded advanced wound dressing in form of in situ forming hydrogel powders: formulation, characterization, and therapeutic potential. Int. J. Biol. Macromol. 274, 133192.
Andredaki, M., Georgoulas, A., Marengo, M., 2020. Numerical investigation of quasi-sessile droplet absorption into wound dressing capillaries. Phys. Fluids 32 (9), 092112.
Browning, M.B., Wilems, T., Hahn, M., Cosgriff-Hernandez, E., 2011. Compositional control of poly(ethylene glycol) hydrogel modulus independent of mesh size. J. Biomed. Mater. Res. A 98A (2), 268–273.
Davies, P., 2012. Exudate assessment and management. Br. J. Community Nurs. 17 (9). Suppl:S18-22, S24.
Domínguez-Robles, J., Cuartas-Gómez, E., Dynes, S., Utomo, E., Anjani, Q.K., Detamornrat, U., Donnelly, R.F., Moreno-Castellanos, N., Larrañeta, E., 2023. Poly (caprolactone)/lignin-based 3D-printed dressings loaded with a novel combination of bioactive agents for wound-healing applications. Sustain. Mater. Technol. 35, e00581.
Dong, R., Guo, B., 2021. Smart wound dressings for wound healing. Nano Today 41, 101290.
Forss, J.R., 2022. Does exudate viscosity affect its rate of absorption into wound dressings? J. Wound Care 31 (3), 236–242.
Gefen, A., Alves, P., Beeckman, D., et al., 2024. Fluid handling by foam wound dressings: from engineering theory to advanced laboratory performance evaluations. Int. Wound J. 21 (2), e14674.
Harries, R.L., Bosanquet, D.C., Harding, K.G., 2016 Sep 1. Wound bed preparation: TIME for an update. Int. Wound J. 13 (S3), 8–14.
Iizaka, S., Sanada, H., Nakagami, G., Koyanagi, H., Konya, C., Sugama, J., 2011. Quantitative estimation of exudate volume for full-thickness pressure ulcers: the ESTimation method. J. Wound Care 20 (10), 453–454, 458–63.
Jones, J., 2015. The thickness of exudate: does it matter? Br. J. Community Nurs. 20 (Sup3), S19–S20.
Joshi, A., Kaur, T., Joshi, A., Gugulothu, S.B., Choudhury, S., Singh, N., 2023. Light-mediated 3D printing of micro-pyramid-decorated tailorable wound dressings with endogenous growth factor sequestration for improved wound healing. ACS Appl. Mater. Interfaces 15, 327–337.
Lan, Z., Kar, R., Chwatko, M., Shoga, E., Cosgriff-Hernandez, E., 2023. High porosity PEG-based hydrogel foams with self-tuning moisture balance as chronic wound dressings. J. Biomed. Mater. Res. A 111 (4), 465–477.
Lustig, A., Alves, P., Call, E., Santamaria, N., Gefen, A., 2021. The sorptivity and durability of gelling fibre dressings tested in a simulated sacral pressure ulcer system. Int. Wound J. 18 (2), 194–208.
Malomuzh, N.P., Bulavin, L.A., Gotsulskyi, V.Y.A., Guslisty, A.A., 2020. Characteristic changes in the density and shear viscosity of human blood plasma with varying protein concentration. Ukr. J. Phys. 65 (2), 151.
Maver, U., Maver, T., 2023. The importance of the correct choice of Franz diffusion cell volume for in vitro drug release testing of wound dressings. Acta Medico-Biotechnica 15 (2), 41–48.
Mellinghoff, A.C., Reininger, A.J., Wurzinger, L.J., Landgraf, R., Hepp, K.D., 1996. Influence of glycemic control on viscosity and density of plasma and whole blood in Type-1 diabetic patients. Diabetes Res. Clin. Pract. 33 (2), 75–82.
Minsart, M., Van Vlierberghe, S., Dubruel, P., Mignon, A., 2022. Commercial wound dressings for the treatment of exuding wounds: an in-depth physico-chemical comparative study. Burns Trauma 10, tkac024.
Neunkirchen, S., Blößl, Y., Schledjewski, R., 2022. A porous capillary tube approach for textile saturation. Compos. Sci. Technol. 230, 109450.
Oh, Y.C., Ong, J.J., Alfassam, H., et al., 2024. Fabrication of 3D printed mutable drug delivery devices: a comparative study of volumetric and digital light processing printing. Drug Deliv. Transl. Res. https://doi.org/10.1007/s13346-024-01697-5 in press.
Op't Veld, R.C., Walboomers, X.F., Jansen, J.A., Wagener, F.A.D.T.G., 2020. Design considerations for hydrogel wound dressings: strategic and molecular advances. Tissue Eng. B Rev. 26, 230–248.
Orlov, A., Gefen, A., 2022. The fluid handling performance of the curea P1 multipurpose dressing against superabsorbent and foam dressing technologies. Int. Wound J. 19 (4), 945–956.
Ramsden, J.J., 2016. Chapter 3 - Forces at the nanoscale. In: Ramsden, J.J. (Ed.), Micro and Nano Technologies, Nanotechnology, Second edition. William Andrew Publishing, pp. 41–60.
Rodríguez-Pombo, L., Xu, X., Seijo-Rabina, A., Ong, J.J., Alvarez-Lorenzo, C., Rial, C., Nieto, D., Gaisford, S., Basit, A.W., Goyanes, A., 2022. Volumetric 3D printing for rapid production of medicines. Addit. Manuf. 52, 102673.
Ruf, M.T., Andreoli, A., Vujic, G., Itin, P., Pluschke, G., Schmid, P., 2017. Exudate collection using wound sponges—an easy, non-invasive and reliable method to explore protease activities in ulcers. Wound Repair Regen. 25, 320–326.
Sánchez-Machado, D.L., Maldonado-Cabrera, A., López-Cervantes, J., Maldonado-Cabrera, B., Chávez-Almanza, A.F., 2023. Therapeutic effects of electrospun chitosan nanofibers on animal skin wounds: a systematic review and meta-analysis. Int. J. Pharm. X 5, 100175.
Santamaria, N., Woo, K., Beeckman, D., Alves, P., Cullen, B., Gefen, A., Lázaro-Martínez, J.L., Lev-Tov, H., Najafi, B., Sharpe, A., Swanson, T., 2023. Clinical performance characteristics for bordered foam dressings in the treatment of complex wounds: an international wound dressing technology expert panel review. Int. Wound J. 20 (9), 3467–3473.
Tickle, J., 2016. Wound exudate: a survey of current understanding and clinical competency. Br. J. Nurs. 25 (2), 102–109.
Townsend, E.C., Cheong, J.Z.A., Radzietza, M., et al., 2024. What is slough? Defining the proteomic and microbial composition of slough and its implications for wound healing. Wound Repair Regen. 1–16.
Tuller, M., Or, D., 2005. Water retention and characteristic curve. In: Hillel, D. (Ed.), Encyclopedia of Soils in the Environment. Elsevier Ltd., Oxford, U.K., pp. 278–289
Vowden, K., Vowden, P., 2003. Understanding exudate management and the role of exudate in the healing process. Br. J. Community Nurs. 8 (Sup5), S4–13.
WUWHS, World Union of Wound Healing Societies, 2007. Principles of Best Practice: Wound Exudate and the Role of Dressings. A Consensus Document. MEP Ltd, London.
Xu, X., Awwad, S., Diaz-Gomez, L., Alvarez-Lorenzo, C., Brocchini, S., Gaisford, S., Goyanes, A., Basit, A.W., 2021. 3D printed punctal plugs for controlled ocular drug delivery. Pharmaceutics 13 (9), 1421.
Xuewu, Z., Xin, L., Dexiang, G., Wei, Z., Tong, X., Yonghong, M., 1996. Rheological models for xanthan gum. J. Food Eng. 27 (2), 203–209.
Zhang, X., Wang, Y., Gao, Z., Mao, X., Cheng, J., Huang, L., et al., 2024. Advances in wound dressing based on electrospinning nanofibers. J. Appl. Polym. Sci. 141 (1), e54746.